Journal of Power Sources 196 (2011) 1378–1385

Contents lists available at ScienceDirect

Journal of Power Sources

journal homepage: www.elsevier.com/locate/jpowsour

Synthesis, structure and electrochemical Li insertion behaviour of $Li_2Ti_6O_{13}$ with the $Na_2Ti_6O_{13}$ tunnel-structure

J.C. Pérez-Flores*, A. Kuhn, F. García-Alvarado

Departamento de Química, Universidad San Pablo-CEU, Urbanización Montepríncipe, Boadilla del Monte, E-28668, Madrid, Spain

ARTICLE INFO

Article history:
Received 28 June 2010
Received in revised form 26 July 2010
Accepted 29 August 2010
Available online 8 September 2010

Keywords:
Lithium ion exchange
Anode material
Electrochemical lithium insertion
Lithium batteries
Lithium secondary battery
Lithium titanium oxide

ABSTRACT

$Li_2Ti_6O_{13}$ has been prepared from $Na_2Ti_6O_{13}$ by Li ion exchange in molten $LiNO_3$ at 325 °C. Chemical analysis and powder X-ray diffraction study of the reaction product respectively indicate that total Na/Li exchange takes place and the Ti–O framework of the $Na_2Ti_6O_{13}$ parent structure is kept under those experimental conditions. Therefore, $Li_2Ti_6O_{13}$ has been obtained with the mentioned parent structure. An important change is that particle size is decreased significantly which is favoring lithium insertion. Electrochemical study shows that $Li_2Ti_6O_{13}$ inserts ca. 5 Li per formula unit in the voltage range 1.5–1.0 V vs. Li^+/Li, yielding a specific discharge capacity of 250 mAh g^{-1} under equilibrium conditions. Insertion occurs at an average equilibrium voltage of 1.5 V which is observed for oxides and titanates where Ti(IV)/Ti(III) is the active redox couple. However, a capacity loss of ca. 30% is observed due to a phase transformation occurring during the first discharge. After the first redox cycle a high reversible capacity is obtained (ca. 160 mAh g^{-1} at C/12) and retained upon cycling. Taking into consideration these results, we propose $Li_2Ti_6O_{13}$ as an interesting material to be further investigated as the anode of lithium ion batteries.

1. Introduction

Research in lithium batteries has focused for years on intercalation or insertion reactions, but more recently new reversible redox reactions involving lithium, for instance alloying, simple metal oxide conversion and reversible extrusion [1] have enlarged the type of materials that can be used to develop lithium batteries. In any case the more recent reports indicate that tailoring crystal morphologies to enable the reaction with lithium has also proved to be an interesting approach to develop new electrode materials. Size reduction to nanometric scale decreases the diffusion length to fully insert the grains at higher current density. A clear example of this approach are titanium oxides, which have received a lot of attention since the influence of crystal size and morphology on electrochemical performances has been reported for several polymorphs [2–5]. This type of results encourages researchers in this field to prepare materials following chemical routes that may produce nanoparticles with controlled morphology or nanostructured electrodes [6].

Lithium titanium oxides such as ramsdellite-type $Li_2Ti_3O_7$ [7], $LiTi_2O_4$ [8] or spinel-type $Li_4Ti_5O_{12}$ [9] and several TiO_2 polymorphs [10–13] have been extensively investigated as insertion electrode materials for rechargeable lithium ion batteries. The electrochemical insertion process that takes place in most of reported lithium titanates and titanium oxides involves partial or full reduction of Ti^{4+} to Ti^{3+} ions at relatively low voltage (ca. 1.5 V) with a specific capacity value under dynamic conditions ranging from 150 to 175 mAh g^{-1} for ramsdellite and spinel materials, respectively. On the other hand, it is already well known that several lithium titanates and titanium oxides suffer very low structural stress upon lithium insertion, characterized by a lack of dimensional change in the structure and the electrode conformation [7,9,14,15]. This *zero strain* behaviour is pointed out as responsible for the long cycle life of such materials [16,17]. In this connection the use of such zero strain materials is interesting for the developing of long life cycling lithium batteries.

Besides titanium oxides and lithium titanates, another series of alkali titanates with general chemical formula $A_2Ti_nO_{2n+1}$ (n = 3–9) have been reported, which can be of interest to develop new electrode materials in view of the open structures provided by the atomic arrangement of oxide ions and Ti(IV). The basic structural motifs of these titanates are corrugated sheets of edge-and corner-sharing Ti–O_6 octahedra. For layered $Na_2Ti_3O_7$ (i.e. n = 3, A = Na) the interlayer spaces are occupied by Na atoms (Fig. 1a). Layered $Li_2Ti_3O_7$ was recently synthesized by ion exchange of Na^+ by Li^+ in $Na_2Ti_3O_7$ [18], and its good electrochemical properties regarding Li intercalation have been highlighted. Note that layered $Li_2Ti_3O_7$ is a metastable polymorph since it cannot be obtained by direct synthesis at high temperature, which leads to the well-known ramsdellite form. The reversible specific capacity delivered is 150 mAh g^{-1}, which is comparable to that of $Li_2Ti_3O_7$ ramsdellite and $Li_4Ti_5O_{12}$ spinel [7,9]. For $A_2Ti_6O_{13}$ (e.g. n = 6), the corrugated

* Corresponding author. Tel.: +34 913724715; fax: +34 913510496.
E-mail address: jcaperez@ceu.es (J.C. Pérez-Flores).

0378-7753/$ – see front matter © 2010 Elsevier B.V. All rights reserved.
doi:10.1016/j.jpowsour.2010.08.106

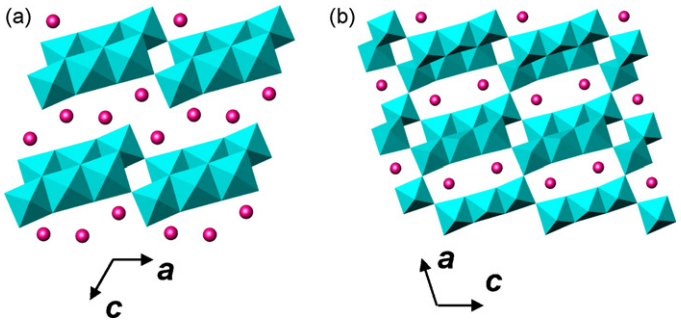

Fig. 1. Schematic representation of the crystal structure of a) $Na_2Ti_3O_7$ and b) $Na_2Ti_6O_{13}$ along the 0 1 0 direction (octahedral: Ti–O_6; spheres: Na).

sheets (that consist of edge- and corner-shared TiO_6 octahedra as above described) are further corner-cross-linked, producing thereby an open tunnel-structure, whose interstitial sites are occupied by the alkali metal Na, K or Rb. A schematic representation of the $Na_2Ti_6O_{13}$ structure is depicted in Fig. 1b. This resembles the structure of TiO_2-B, which is obtained by heating a hydrated protonated layered tetratitanate with composition $KHTi_4O_9$ to 500 °C [12]. Recently, nanowires of TiO_2-B has shown to develop a specific reversible capacity of 200 mAh g^{-1} at 1.5 V at very high rate [19]. Such results encourage research on related structures to seek for new related materials with improved capacity to insert lithium reversibly.

$Na_2Ti_6O_{13}$ has been shown to undergo reversible electrochemical Li insertion and de-insertion reactions [20,21]. Ion exchange in molten Li salts was used to obtain $Li_2Ti_6O_{13}$ from $K_2Ti_6O_{13}$ or $Na_2Ti_6O_{13}$ [22]. However, it was not further characterized, neither structurally nor regarding its electrochemical lithium insertion properties.

In this work we have synthesized $Li_2Ti_6O_{13}$ by ion exchange of Na^+ by Li^+ in $Na_2Ti_6O_{13}$. The as-obtained lithium titanate is structurally characterized by Rietveld analysis of X-ray powder data. Furthermore, we have analyzed the electrochemical lithium insertion and de-insertion properties of $Li_2Ti_6O_{13}$ to asses its possible use as negative electrode for rechargeable Li batteries.

2. Experimental

The precursor $Na_2Ti_6O_{13}$ was prepared by two different routes. The first route used an already reported solid state reaction [23]; stoichiometric amounts of Na_2CO_3 (99.95%, Aldrich) and rutile TiO_2 (99.99%, Aldrich) were mixed and ground in a mortar. The mixture was heated to 800 °C for decomposition of the carbonate. After regrinding, the mixture was pelletized and heated to 925 °C for 36 h in air. The second route comprised a modified sol–gel method [24]; a 1:1 solution of $Ti(C_4H_9O)_4$ (ρ = 0.881 g ml^{-1}, Aldrich) in 1-butanol (ρ = 0.81 g ml^{-1}, Scharlau) containing the stoichiometric amount of titanium was drop-wisely added to a 1 M NaOH aqueous solution. The addition was made under continuous stirring in order to get a fast hydrolysis–condensation reaction. After mixing was completed, the resulting solution was heated at 100 °C until the gel formed as a suspension. Afterwards, it was completely dried by freeze-drying (2 days at 0.005 mbar and −49 °C). The powder obtained was ground and heated at 925 °C for 36 h in air.

$Li_2Ti_6O_{13}$ was prepared from $Na_2Ti_6O_{13}$ by ion exchange of Na^+ by Li^+ carried out at mild temperatures using a molten lithium salt. A 100% excess of $LiNO_3$ with respect to the stoichiometric quantity was mixed with $Na_2Ti_2O_{13}$ and pelletized. Pellets were heated at 325 °C in air during 4 days. Then, the resulting product was crushed, washed with distilled water and the remaining white solid $Li_2Ti_6O_{13}$ filtered through 2 μm pore-size filter paper.

The ion-exchange rate was calculated by determining the sodium content in the filtered solution, as a 1 Na^+ by 1 Li^+ exchange is assumed. Analysis of Na content was carried out by means of flame atomic emission spectroscopy, using a Sherwood 410 flame photometer and a standard sodium solution ([Na^+] = 1000 ppm in HNO_3, Fluka).

Structural characterization was made using powder X-ray diffraction (PXRD) in reflection mode. Diffraction patterns were recorded on a X'Pert PRO PANalytical diffractometer, operating at 45 kV and 40 mA, equipped with a hybrid monochromator, working with Cu $K_{\alpha 1}$ (λ = 1.54056 Å) radiation and a Bruker AXS' LynxEye detector. Diffraction patterns were analyzed and crystal structures determined by Rietveld [25,26] analysis with the FullProf software [27] in the angular range 2θ = 10–100°. Crystal symmetry was in addition studied by means of Selected Area Electron Diffraction (SAED) with a JEOL 2000FX electron microscope, which include an OXFORD INCA EDS detector allowing for chemical microanalysis.

On the other hand, the morphology of crystallites obtained was determined by Scanning Electron Microscopy using a JEOL JSM-6400 microscope. Pellets and powders were sputtered with gold as conductive coating and images were recorded while operating at 20 kV and 15 nm as working distance.

Electrochemical lithium insertion/de-insertion experiments were performed using lithium coin-type CR2032 cells, accordingly to the following general configuration:

$$(-)Li//LiPF_6 \text{ in EC + DMC}//Li_2Ti_6O_{13} + C + \text{Kynarflex}(+)$$

A lithium metal disk (5 mm diameter) was used as the anode. The composite cathode was made by mixing 60% $M_2Ti_6O_{13}$ (M = Na or Li) as active material, 35% carbon black (Cabot Corp.) and 5% Kynarflex as binder (Elf Atochem) in weight by pressing the resulting mixture into 8 mm diameter pellets having ca. 11 mg active material. A solution of 1 M $LiPF_6$ in a 50:50 mixture of ethylene carbonate (EC) and dimethyl carbonate (DMC) by volume was used as the electrolyte (Selectipur LP30, Merck). Cells were assembled in an argon-filled glove box and run and controlled by using a multichannel MacPile II system (BioLogic). Galvanostatic experiments were carried out under different C/n rates, where n stands for the time needed (in hours) to insert 1 lithium per formula weight of titanate. Experiments close to equilibrium were carried out using the galvanostatic intermittent titration technique, GITT, with current density pulses of 0.1 mA cm^{-2}, which were applied for 30 min. After each pulse, current was switched off and the system was allowed to relax for 12 h in order to reach equilibrium before applying the next pulse.

3. Results and discussion

3.1. Synthesis

Both synthetic procedures described in the experimental section to prepare $Na_2Ti_6O_{13}$ yielded white powders, whose XRD pattern could be indexed in the monoclinic system and space group C2/m, accordingly to the structure reported for $Na_2Ti_6O_{13}$ [23]. A small fraction of rutile as a secondary phase was commonly present, independently on the preparation route used. Refined lattice parameters for the two samples of precursor $Na_2Ti_6O_{13}$ prepared are listed in Table 1. Note that lattice parameters are practically the same regardless the synthetic method. Besides, these values are in good agreement with those previously reported by other authors (see Table 1).

X-ray diffraction patterns of starting $Na_2Ti_6O_{13}$ and ion-exchanged $Li_2Ti_6O_{13}$ are shown in Fig. 2 where no significant changes can be seen. The lattice parameters of both starting $Na_2Ti_6O_{13}$ and ion-exchanged $Li_2Ti_6O_{13}$ obtained are listed in

Table 1
Refined lattice parameters for $Na_2Ti_6O_{13}$ and $Li_2Ti_6O_{13}$.

Compound	a (Å)	b (Å)	c (Å)	β (°)	V (Å^3)
$Na_2Ti_6O_{13}$ (this work: ceramic)	15.10999(27)	3.74641(5)	9.17368(16)	99.01527(99)	512.89(2)
$Na_2Ti_6O_{13}$ (this work: freeze-dried)	15.1075(4)	3.74474(8)	9.1735(2)	99.031(3)	512.54(2)
$Na_2Ti_6O_{13}$ Ref. [28]	15.095(7)	3.745(3)	9.174(1)	99.01	512.214
$Na_2Ti_6O_{13}$ Ref. [23]	15.131(2)	3.745(2)	9.159(2)	99.30(5)	512.178
$Li_2Ti_6O_{13}$ (this work: ion exchange)	15.3457(7)	3.7527(1)	9.1528(2)	99.466(2)	519.92(3)
$Li_2Ti_6O_{13}$ Ref. [22]	15.45(2)	3.757(2)	9.11(2)	99.8	521.080

Table 1. In comparison with $Na_2Ti_6O_{13}$ the a-axis length and unit cell volume increase, while the c-axis slightly decreases. This fact must be evidently a consequence of the exchange of the large Na^+ by the smaller Li^+ ions. Our lattice parameters are in fair agreement with those reported by England et al. [22], with little deviations in a and c parameters with respect to the previous reported. They found that the cell volume of resulting $Li_2Ti_6O_{13}$ was anomalous; it was indeed larger than that of $Na_2Ti_6O_{13}$, which after them indicated that Li^+ ions are occupying a position with lower coordination and that removal of sodium was not likely completed. When compared to our sample the differences found may indicate that the different experimental conditions used to carry out the exchange reactions produced samples with different Na/Li content. In our case the chemical analysis of Na^+ in the filtrate solution confirmed that the Na^+ for Li^+ ion exchange was quantitative. Therefore, the lithium titanate herein described is formulated as $Li_2Ti_6O_{13}$.

3.2. Structure refinement

X-ray patterns of $Li_2Ti_6O_{13}$ suitable for Rietveld refinement were obtained in reflection mode. The morphology and microstructure was after analyzed by means of SEM and ED (see below). The crystal structure of $Li_2Ti_6O_{13}$ was refined using starting $Na_2Ti_6O_{13}$ as initial structural model.

During the refinement, the site occupations of the atoms were fixed to 1.0. Furthermore, the thermal B factors were constrained for atoms of a given type and, therefore refined to the same value for each atom type. Fig. 3 shows the observed, calculated and the difference patterns for the Rietveld refinement of $Li_2Ti_6O_{13}$. Refined atomic coordinates are given in Table 2 and selected interatomic distances are listed in Table 3.

The basic structural $Ti_6O_{13}{}^{2-}$ motif in $Li_2Ti_6O_{13}$, consisting of blocks of three edge-sharing TiO_6 octahedra, remains mainly unchanged in comparison to the starting $Na_2Ti_6O_{13}$. All TiO_6 octahedra are clearly distorted, having average Ti–O distances ranging from 1.998 to 2.037 Å. These values are consistent with those observed in $Na_2Ti_6O_{13}$ [23].

At the initial stage of refinement, Li was placed on the unique Na site present in the starting $Na_2Ti_6O_{13}$ structure. In this the Na site is surrounded by eight nearest oxygen atoms in a distorted cubic arrangement [23]. Obviously, this site seems to be unstable to be occupied by Li atoms. Although the refinement did not allow to

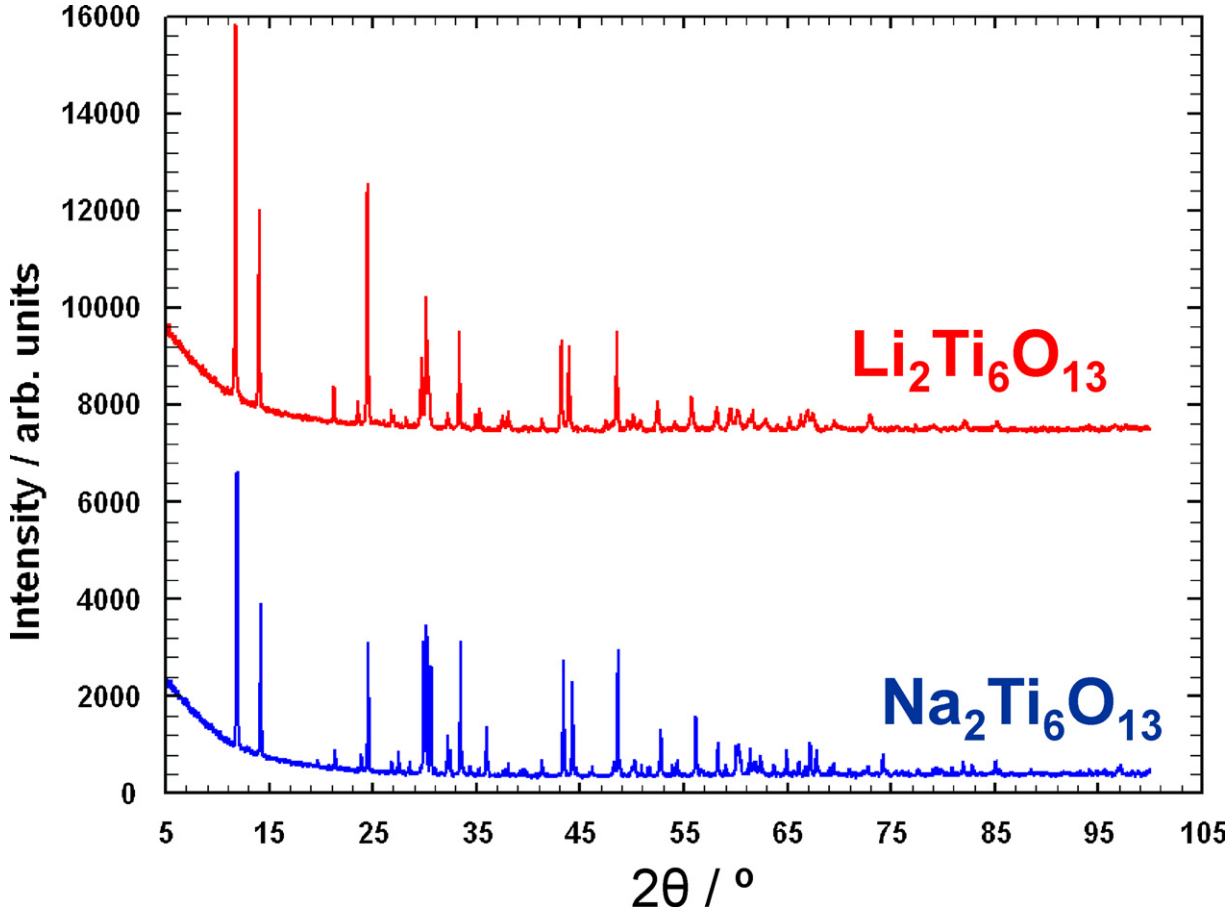

Fig. 2. Powder X-ray diffraction patterns of $Na_2Ti_6O_{13}$ obtained by sol–gel and $Li_2Ti_6O_{13}$ prepared from the former by Na^+/Li^+ ion-exchange reaction.

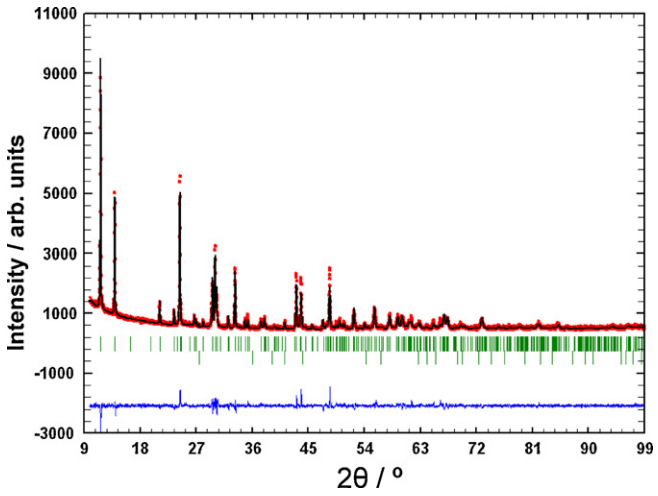

Fig. 3. Observed (points), calculated (solid line) and difference (bottom) patterns for the Rietveld analysis from powder X-ray data of $Li_2Ti_6O_{13}$. The vertical bars indicate the peak positions of all allowed Bragg reflections. The secondary TiO_2 phase is shown too.

Table 2
Structural parameters of $Li_2Ti_6O_{13}$ determined from XRD data.[a]

Atom	Site	x	y	z	B (Å²)[b]	Occupancy
Li1	4i	0.52(20)	0	0.39(36)	2.0(0)	1.0
Ti1	4i	0.1139(3)	0	0.0914(7)	2.0(1)	1.0
Ti2	4i	0.1643(4)	0	0.4331(9)	2.0(1)	1.0
Ti3	4i	0.2299(4)	0	0.7742(7)	2.0(1)	1.0
O1	2a	0	0	0	0.0 (1)	0.5
O2	4i	0.243(1)	0	0.244(2)	0.0 (1)	1.0
O3	4i	0.060(1)	0	0.291(2)	0.0 (1)	1.0
O4	4i	0.303(1)	0	0.572(2)	0.0 (1)	1.0
O5	4i	0.124(1)	0	0.618(2)	0.0 (1)	1.0
O6	4i	0.3587(9)	0	0.890(1)	0.0 (1)	1.0
O7	4i	0.151(1)	0	0.894(2)	0.0 (1)	1.0

[a] Crystal data: chemical formula $Li_2Ti_6O_{13}$, monoclinic, space group: C2/m, refined lattice parameters: $a = 15.3457(7)$ Å, $b = 3.7527(1)$ Å, $c = 9.1528(2)$ Å, $\beta = 99.466(2)^\circ$. Reliability factors: $R_{wp} = 5.74\%$, $R_p = 4.35\%$, $R_e = 3.87\%$, $R_F = 4.72\%$, $R_B = 7.50\%$, $\chi^2 = 2.21$
[b] B parameters were constrained for atoms of a given type.

Table 3
Selected bond distances (Å) for $Li_2Ti_6O_{13}$.

Ti1–O1	1.811(6)		
Ti1–O2	2.23(1)		
Ti1–O3	2.13(2)		
Ti1–O6 × 2	1.924(3)		
Ti1–O7	1.97(2)	Mean Ti1–O	1.998
Ti2–O2	2.26(2)		
Ti2–O3	1.882(1)		
Ti2–O4	2.29(1)		
Ti2–O4 × 2	1.944(5)		
Ti2–O5	1.90(2)	Mean Ti2–O	2.037
Ti3–O2 × 2	1.934(5)		
Ti3–O4	2.32(3)		
Ti3–O5	1.966(1)		
Ti3–O6	2.085(1)		
Ti3–O7	1.769(2)	Mean Ti3–O	2.001

accurately locate the position of the light Li using X-ray diffraction, based on the fractional coordinates $x = 0.52$, $y = 0.0$, $z = 0.39$ obtained, Li seems to shift towards a more central position within the tunnel, where a lower fourfold coordination is obtained for the smaller Li atom, with Li–O distances ranging from 2.0 to 2.4 Å (see Fig. 4). In any case, neutron diffraction experiments are planned for a more accurate determination of the lithium distribution and occupation.

3.3. Electron microscopy study

A morphological effect of the ion-exchange reaction can be seen in the SEM images shown in Fig. 5a and b; they correspond to $Na_2Ti_6O_{13}$ and $Li_2Ti_6O_{13}$ respectively. To obtain a better resolution, as prepared samples were pressed to pellets and treated a few hours at the synthesis temperature. We checked that this thermal treatment did not change particle size but it improved the quality of images recorded. It can be seen that particles of parent $Na_2Ti_6O_{13}$ are larger than those of the exchanged product $Li_2Ti_6O_{13}$; one possible reason might be related to the internal structural stress due to the change in the cell parameters and volume upon the ion-exchange reaction. In the former a very inhomogeneous distribution of particle size is observed within an 8–10 μm range. In the latter, particle size distribution seems to be more homogeneous with an average size ranging from 0.5 to 0.8 μm. Therefore the exchanged product has been obtained as sub-micrometric particles that may facilitate insertion reaction of lithium.

A more detailed view of the morphology and microstructure of both $Na_2Ti_6O_{13}$ and $Li_2Ti_6O_{13}$ has been obtained by means of Transmission Electron Microscopy combined with Selected Area Electron Diffraction. The lattice spots observed in selected area diffraction (SAED) patterns of $Na_2Ti_6O_{13}$ and $Li_2Ti_6O_{13}$ samples are compatible with the C2/m monoclinic space group, using as cell parameters: $a \approx 15.1$ Å, $b \approx 3.8$ Å, $c \approx 9.2$ Å and $\beta \approx 99^\circ$ for $Na_2Ti_6O_{13}$ and $a \approx 15.3$ Å, $b \approx 3.8$ Å, $c \approx 9.1$ Å and $\beta \approx 99^\circ$ for $Li_2Ti_6O_{13}$ [22].

As an example, Fig. 6 shows two selected zone axis for a thin crystal of each compound and a TEM image (Fig. 6a and d) corresponding to the zone axis [−1 1 0] shown in Fig. 6b and e, and zone axis [1–30] and [−1 1 1] in Fig. 6c and f, respectively. It can be seen that the preferred growing direction of the parent is [1 1 0], contrarily to that observed by Dominko et al. [21]. As a result of the topotactic reaction the Li-exchanged derivative exhibits the same morphology though, as aforementioned, crystal size has considerably decreased. Therefore, we expect that this particular change of size favors insertion of lithium into the Li-exchanged material to give an improved positive electrode for lithium cells.

EDS measurements have been carried out on several thin crystals corresponding to the sodium and lithium titanates to verify the ion-exchange rate achieved. Results showed that every crystal of $Na_2Ti_6O_{13}$ has a similar Na/Ti ratio of 1/3, whereas for $Li_2Ti_6O_{13}$ this ratio was found to be zero for every crystal analyzed. These results indicate that total lithium exchange was achieved, in agreement also with the results from chemical analysis given in Section 3.1.

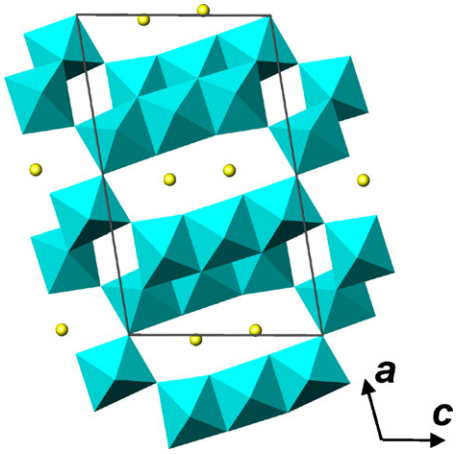

Fig. 4. Schematic representation of the crystal structure of $Li_2Ti_6O_{13}$. Ti atoms are centred by oxygen atoms in a distorted octahedral environment. These are corner-linked to form triple blocks of edge-sharing Ti–O_6 octahedra. Li atoms are shown as spheres.

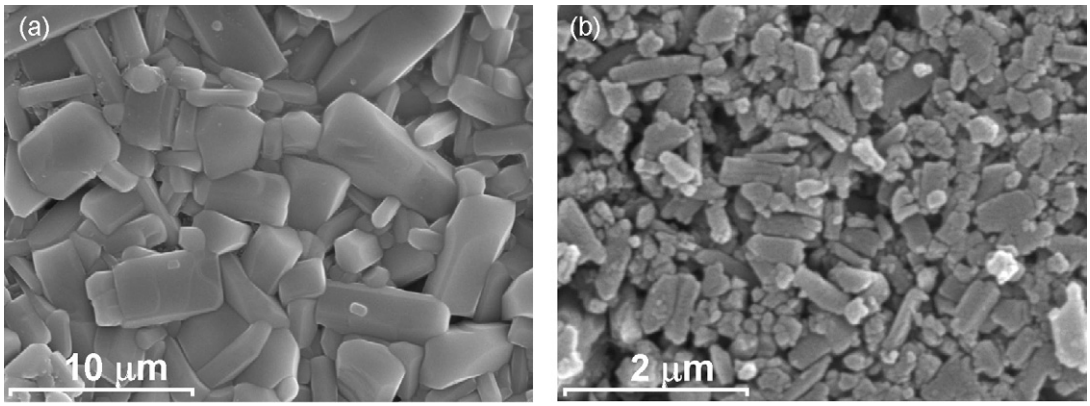

Fig. 5. SEM micrographs of surface pellets of as prepared $Na_2Ti_6O_{13}$ a) and $Li_2Ti_6O_{13}$ b).

3.4. Electrochemical properties

For a better assessment of the possible advantages of $Li_2Ti_6O_{13}$ with respect to $Na_2Ti_6O_{13}$ the main electrochemical characteristics of the latter will be also briefly presented. Further details on the electrochemical Li insertion chemistry of $Na_2Ti_6O_{13}$ can be found in previously reported works [20,21].

Fig. 7 shows a typical voltage–composition plot as well as the incremental capacity between 3.0 and 0.8 V for the first discharge of two cells bearing $Na_2Ti_6O_{13}$ (Fig. 7a) and $Li_2Ti_6O_{13}$ (Fig. 7b), respectively, as electroactive material and run at C/12 (1 Li per formula unit every 12 h, 0.1 mA cm^{-2} or 4.5 μA mg^{-1}). It can be seen in the *E–x* curve that Li insertion into $Na_2Ti_6O_{13}$, produces three pseudo plateaus in the voltage range 1.5–0.8 V, which are better seen as maxima in the incremental capacity curve (labelled as I'_{Na} to III'_{Na}). These quasi constant-voltage regions can be assigned to biphasic regions (I_{Na}, II_{Na} and III_{Na}) at 1.32, 1.11 and 0.90 V, respectively. In between the biphasic regions, single phases are detected as minima in the incremental capacity curve. Since we have found that only the first and second processes are reversible, we are discussing only the voltage range 3.0–1.0 V. The process at 1.32 V is typical for the Ti(IV) to Ti(III) reduction, since approximately the same value has been observed in most of electroactive titanates and titanium (IV) oxides [20,28,29]. The second process occurring at 1.11 V should be also related to the reduction of the transition metal, although we cannot confirm any information relative to the operating redox couple state. Under the galvanostatic conditions used for the experiment shown in Fig. 7 ca. 3 Li atoms per formula unit are inserted into sodium titanate down to 1.0 V. The corresponding specific discharge capacity in this voltage range is 150 mAh g^{-1}, which is in agreement with the values reported previously by Dominko et al. [20,21].

When the above described insertion behaviour is compared to that observed for $Li_2Ti_6O_{13}$ (see the corresponding first discharge in Fig. 7b), significant differences can be found. In this case only two pseudo plateaus appear in the voltage range 3.0–0.8 V, and the one at higher voltage is significantly longer. Again the process at low voltage, appearing below 0.9 V in this case, is irreversible as we are showing below. Accordingly to the same interpretation made for the $Na_2Ti_6O_{13}$, the first pseudo constant-voltage regions (I_{Li}) has been assigned to a biphasic regions where Ti(IV) is being reduced to Ti(III). This process is easily identified as a maximum (I'_{Li}) in the incremental capacity curve at 1.45 V and parallels that observed for the sodium compound at similar voltage. A clear

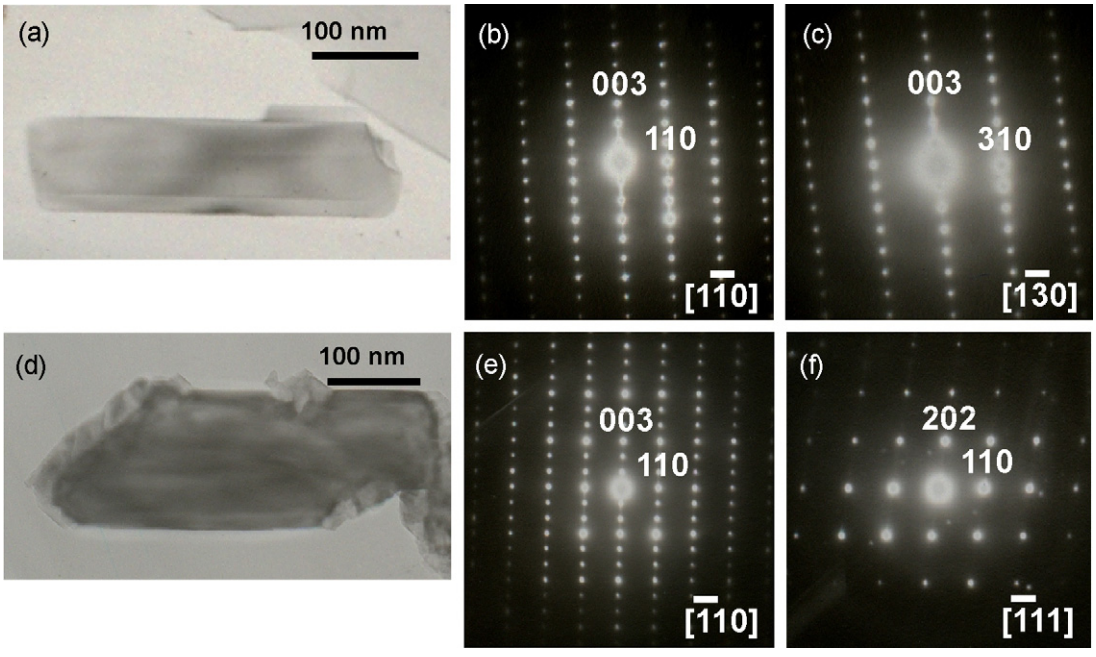

Fig. 6. Low magnification TEM images of a) $Na_2Ti_6O_{13}$ and d) $Li_2Ti_6O_{13}$. Two typical SAED patterns are also shown for both $Na_2Ti_6O_{13}$ (b and c) and $Li_2Ti_6O_{13}$ (e and f).

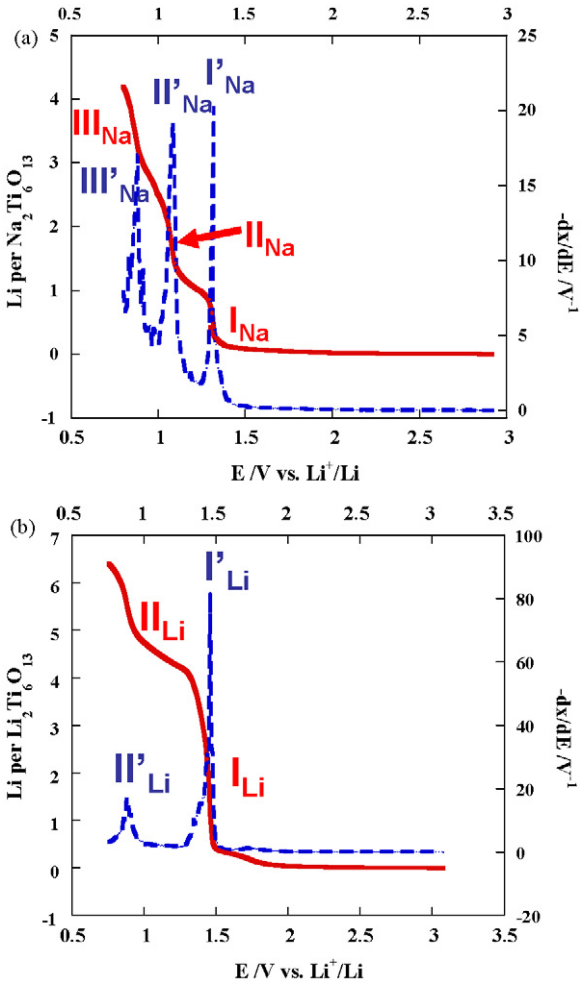

Fig. 7. Incremental capacity (dashed line) and composition (continuous line) vs. voltage for two cells bearing a) $Na_2Ti_6O_{13}$ and b) $Li_2Ti_6O_{13}$ as the positive electrode. Cells were discharged at C/12 (0.1 mA cm^{-2} or 4.5 μA mg^{-1}). Two-phase regions are marked as I_M, II_M and III_M in the voltage–composition curve and as I'_M, II'_M and III'_M in the incremental capacity ones (M = Na or Li).

difference between the two titanates is that the process found at the intermediate voltage 1.11 V in $Na_2Ti_6O_{13}$ is not observed in $Li_2Ti_6O_{13}$. The first discharge down to 0.9 V proceeds up to ca. 5 Li/formula $Li_2Ti_6O_{13}$, yielding a specific capacity of approximately 250 mAh g^{-1}.

Fig. 8 illustrates the first discharge–charge cycle in the voltage region 3.0–1.0 V for each of the investigated titanate as well as the variation of reversible cell capacity with the number of cycles. In both cases cells were run at C/12 (±0.1 mA cm^{-2} or 4.6 μA mg^{-1}).

The voltage–composition curves (Fig. 8a) show clearly differentiated profiles. The shape for $Na_2Ti_6O_{13}$ is maintained on charge, a clear indication of the reversibility of the insertion reaction. However, ca. 19% capacity loss is observed on charging since the first charge capacity is 140 mAh g^{-1}. Further cycling is shown in Fig. 8b where it can be seen that a specific capacity of around 100 mAh g^{-1} is stabilized after the first few cycles, equivalent to the insertion–de-insertion of ca. 2 Li ions, similarly to data previously reported [20].

For $Li_2Ti_6O_{13}$ it can be seen in Fig. 8a that under the same experimental conditions the first discharge capacity is higher than that of $Na_2Ti_6O_{13}$, though the maximum theoretical capacity assuming full reduction of Ti(IV), i.e. that corresponding to insertion of 6 Li/formula unit, is reached in none of them.

When $Li_2Ti_6O_{13}$ cells are discharged at C/12 down to 1.0 V (Fig. 8a) which is just before reaching region II_{Li} (see Fig. 7), 4.8 lithium atoms are inserted and almost 75% of them can be de-inserted on charge. Note that while the charge curve of $Na_2Ti_6O_{13}$ develops exactly the same shape as the discharge curve, for $Li_2Ti_6O_{13}$ the charge curve is clearly different, since the almost perfect plateau observed on the discharge deviates to a regime with a more continuous variation of voltage vs. time. This may indicate either a limited kinetics of oxidation or an irreversible phase transformation in region I_{Li} (see Fig. 7). However, further cycling shows that after the first discharge the de-insertion/insertion process is highly reversible. After the initial cycles, a reversible specific capacity of 160 mAh g^{-1} is obtained, and this value is kept upon further cycling. Note that the reversible capacity is significantly higher than that observed for $Na_2Ti_6O_{13}$.

On the other hand, the first and second discharge of $Li_2Ti_6O_{13}$ as the positive electrode of cells discharged at different current rates can be seen in Fig. 9. For comparative purposes all cells have been discharged to 1.0 V, in order to be sure that region II_{Li} is not reached and that the only operating mechanism is the reduction of Ti(IV) to Ti(III). It can be seen that cells are able to sustain a discharge rate of up to 1C (i.e. insertion of 1 Li every 1 h) while keeping a capacity of 100 mAh g^{-1}.

The electrochemical data shown point to $Li_2Ti_6O_{13}$ as an interesting material to anode in lithium batteries that deserves to be

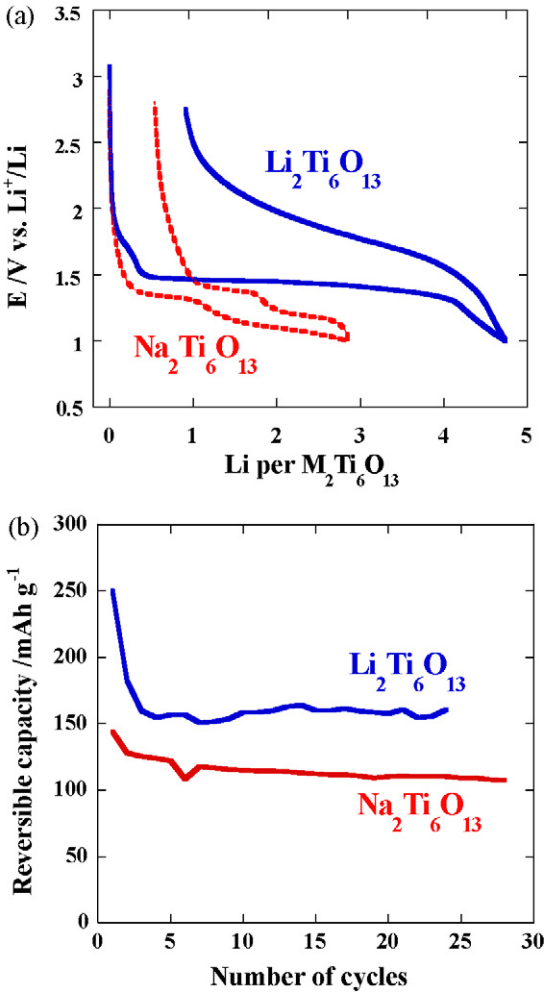

Fig. 8. a) Voltage–composition curve and b) reversible specific capacity in the range 3.0–1.0 V with a C/12 rate for $Li_2Ti_6O_{13}$ (continuous line) and for $Na_2Ti_6O_{13}$ (dashed line).

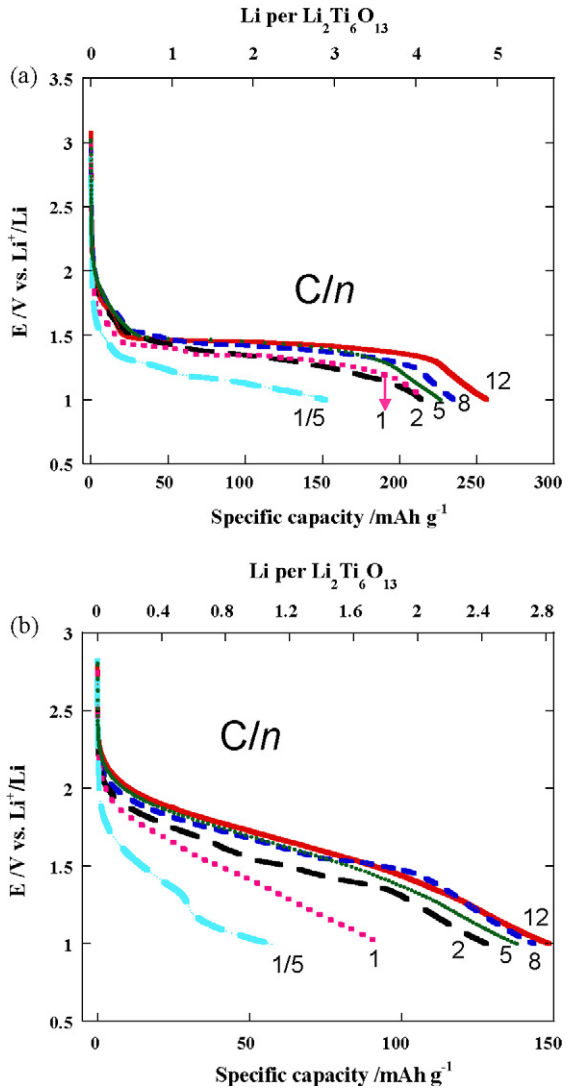

Fig. 9. Specific capacity developed in the a) first and b) second discharge for Li//$Li_2Ti_6O_{13}$ cells down to 1.0 V at different C/*n*.

further investigated in order to optimize electrode processing and to understand the insertion mechanism.

Electrochemical insertion of lithium in the 3.0–1.0 V range has been also investigated by means of GITT experiment under isothermal conditions (25 °C) in order to asses the maximum quantity of Ti(IV) that can be reduced to Ti(III) accordingly to the ideal reaction:

$$Li_2(Ti^{4+})_6O_{13} + 6e^- + 6Li^+ \rightarrow Li_8(Ti^{+3})_6O_{13}$$

Fig. 10 shows the first discharge of a cell from its rest potential (ca. 3.0 V) to 1.4 V (curve a). The lower cut off voltage has been increased from 1.0 to 1.4 in as much as GITT conditions minimize polarization effects. In fact, Fig. 10, (curve b) shows a similar cell but discharged at 1.2 V under equilibrium. It can be seen that no more than 5.5 lithium ions can be reversibly inserted, even though equilibrium is reached in every step under the GITT conditions given in the experimental section. Besides, it can be now clearly seen that the process occurring at lower voltage (labelled II_{Li} in Fig. 7) does not contribute to the reversible capacity. On the other hand, Fig. 10 shows that even under equilibrium the two-phase transformation occurring at 1.5 V during the first discharge is not reversible, since the shape of voltage–composition curve of discharge and charge are different in spite of that kinetics effect are minimized under GITT conditions. This means that the very first lithium atoms that are inserted transform the structure of $Li_2Ti_6O_{13}$ that can afterwards insert and de-insert lithium reversibly.

A tentative explanation of the differences observed in the electrochemical behaviour of both titanates, e.g. concerning the number of insertion processes, will be given hereafter. Based on the electrochemical results we can conclude that $Na_2Ti_6O_{13}$ undergoes a real topotactical Li insertion reaction with retention of the skeleton Ti–O framework structure. The Li insertion occurs in two stages with current peaks located at 1.3 and 1.1 V, in agreement with previous reports [20,21]. Then, the presence of two energetically different insertion processes developed at different insertion voltages are likely related to the occupation of energetically different sites for Li within the $Na_2Ti_6O_{13}$ structure. For $Li_2Ti_6O_{13}$, however, the single narrow current peak present in the first discharge and located at ca. 1.5 V is probably due to a structural phase transformation of the starting skeleton structure. An analysis of the incremental capacity vs. voltage plot over several cycles showed that the electrochemical behaviour of the lithium titanate after the first discharge (i.e. first charge and following discharge–charge cycles) is governed by a broad peak that shifted to higher 1.7 V. This peak is perfectly maintained over numerous cycles, reflecting the excellent cyclability of the lithium titanate. We are actually studying the nature of the Li insertion mechanisms into $Na_2Ti_6O_{13}$ and $Li_2Ti_6O_{13}$ by means of neutron diffraction. Detailed results will be published elsewhere.

We have shown that lithium reacts with $Li_2Ti_6O_{13}$ at 1.5 V under equilibrium conditions which corresponds to the thermodynamic equilibrium voltage for the reduction process Ti(IV)/Ti(III) in this oxide. This reduction voltage is lower than those expected for Ti(IV) located in TiO_6 octahedron, which have been reported in the range of 1.8–1.6 V vs. lithium [10,30], but it is in concordance with other previous results involving similar materials and structures [9,20,28,29]. Besides, the insertion process involves ca. 5 lithium atoms per $Li_2Ti_6O_{13}$ developing a capacity of 250 mAh g^{-1}, which is equivalent to ca. 0.8 Li ion per Ti atom. This figure is then significantly higher than the commonly accepted 0.5 Li/Ti atom, approaching the values reported for recent improvements in titanium oxides [19,20,31]. However, a capacity loss of ca. 30% is observed during the first discharge likely due to a phase transformation.

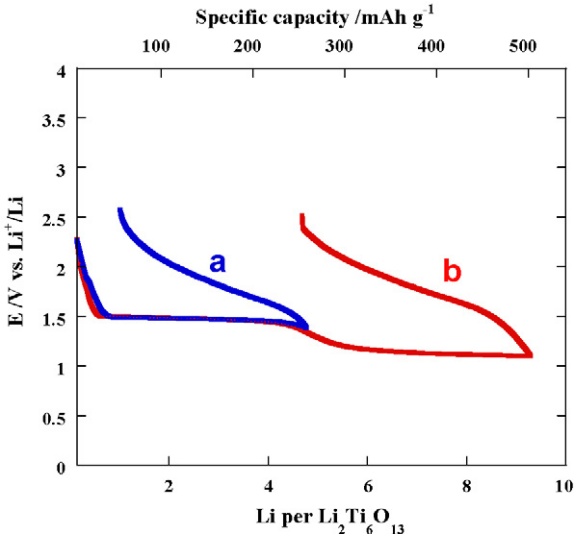

Fig. 10. GITT measurements on Li//$Li_2Ti_6O_{13}$ cells at ±0.1 mA cm^{-2} for 30 min every 12 h and discharged down to a) 1.4 or b) 1.2 V. Cells were allowed to relax for 12 h after each current pulse.

In view of the results presented above the ion exchange of Na^+ by Li^+ ions in $Li_2Ti_6O_{13}$ seems to be a way to improve electrochemical performances of $Na_2Ti_6O_{13}$. $Li_2Ti_6O_{13}$ is able to react with more lithium atoms and even though capacity loss after the first discharge is higher, the reversible capacity of electrodes based on $Li_2Ti_6O_{13}$ (160 mAh g^{-1} at C/12) is greater than for $Na_2Ti_6O_{13}$ (100 mAh g^{-1} at C/12). Therefore, $Li_2Ti_6O_{13}$ is worth being further investigated as a new titanium based anode for rechargeable lithium batteries [32]. Note that some preliminary performances of this new material are at least comparable to other titanium oxides commonly used nowadays and accepted like current *state-of-art*. For example, $Li_4Ti_5O_{12}$ spinel [33,34] and $Li_2Ti_3O_7$ ramsdellite [7,18] yield a reversible capacity of 160 mAh g^{-1}, a value which is also sustained for many cycles at C/12 using $Li_2Ti_6O_{13}$ as the positive electrode.

Structural and chemical changes associated to the reduction of Ti(IV) to Ti(III) in $Li_2Ti_6O_{13}$ are presently being analyzed using neutron diffraction data of chemical intercalated samples. Results will be reported elsewhere.

4. Conclusions

Lithium ion-exchange has been carried out on $Na_2Ti_6O_{13}$ to yield a fully exchanged Na/Li derivative with composition $Li_2Ti_6O_{13}$. The main structural characteristics of the parent $Na_2Ti_6O_{13}$ are maintained in $Li_2Ti_6O_{13}$, though important morphological changes have been found. Average particle size of $Li_2Ti_6O_{13}$ is much smaller, which favors electrochemical insertion in such insulating oxides.

Insertion of lithium into $Li_2Ti_6O_{13}$ occurs at an average voltage of 1.5 V, which is characteristic of the Ti(IV)/Ti(III) redox couple. The reaction proceeds through a two-phase reaction involving ca. 5 lithium ions/formula unit. Afterwards, the new phase which is likely related to $Li_2Ti_6O_{13}$, reversibly de-inserts and inserts lithium. Though under equilibrium conditions the capacity developed in the first discharge is ca. 250 mAh g^{-1}, a capacity loss of ca. 30% is observed due to a phase transformation occurring during the first discharge. After the first redox cycle a high reversible capacity is obtained (160 mAh g^{-1} at C/12) and retained upon cycling. This reversible capacity is similar to that obtained for other titanium oxides that have been already proposed as the anode for lithium rechargeable batteries (e.g. spinel $Li_4Ti_5O_{12}$, ramsdellite $Li_2Ti_3O_7$). Therefore we propose $Li_2Ti_6O_{13}$ as a new candidate to anode material that is worth being further investigated to optimize electrochemical performances and to understand fundamental aspects of the insertion reaction.

Acknowledgements

We thank Ministerio de Educación y Ciencia and Comunidad de Madrid for funding the projects MAT2007-64486-C07-01 and S2009/PPQ-1626 respectively. Financial support from Universidad San Pablo is also acknowledged.

References

[1] J.M. Tarascon, M. Armand, Nature 414 (2001) 359–367.
[2] L. Kavan, M. Gratzel, Electrochemical and Solid-State Letters 5 (2002) A39–A42.
[3] S.R.S. Prabaharan, M.S. Michael, H. Ikuta, Y. Uchimoto, M. Wakihara, Solid State Ionics 172 (2004) 39–45.
[4] A.R. Armstrong, G. Armstrong, J. Canales, R. García, P.G. Bruce, Advanced Materials 17 (2005) 862–865.
[5] G. Armstrong, A.R. Armstrong, J. Canales, P.G. Bruce, Chemical Communications (2005) 2454–2456.
[6] D. Tonti, M.J. Torralvo, E. Enciso, I. Sobrados, J. Sanz, Chemistry of Materials 20 (2008) 4783–4790.
[7] M.E.A.Y. de Dompablo, E. Morán, A. Várez, F. García-Alvarado, Materials Research Bulletin 32 (1997) 993–1001.
[8] A. Kuhn, C. Baehtz, F. García-Alvarado, Journal of Power Sources 174 (2007) 421–427.
[9] T. Ohzuku, A. Ueda, N. Yamamoto, Journal of the Electrochemical Society 142 (1995) 1431–1435.
[10] B. Zachau-Christiansen, K. West, T. Jacobsen, S. Atlung, Solid State Ionics 28–30 (1988) 1176–1182.
[11] D.W. Murphy, R.J. Cava, S.M. Zahurak, A. Santoro, Solid State Ionics 9–10 (1983) 413–417.
[12] R. Marchand, L. Brohan, M. Tournoux, Materials Research Bulletin 15 (1980) 1129–1133.
[13] M.A. Reddy, M.S. Kishore, V. Pralong, U.V. Varadaraju, B. Raveau, Electrochemical and Solid-State Letters 10 (2007) A29–A31.
[14] A. Kuhn, R. Amandi, F. García-Alvarado, Journal of Power Sources 92 (2001) 221–227.
[15] M.E. Arroyo, Y. de Dompablo, A. Várez, F. García-Alvarado, Journal of Solid State Chemistry 153 (2000) 132–139.
[16] M.M. Thackeray, Journal of the Electrochemical Society 142 (1995) 2558–2563.
[17] G.G. Amatucci, F. Badway, A.D. Pasquier, T. Zheng, Journal of the Electrochemical Society 148 (2001) A930–A939.
[18] K. Chiba, N. Kijima, Y. Takahashi, Y. Idemoto, J. Akimoto, Solid State Ionics 178 (2008) 1725–1730.
[19] A.R. Armstrong, G. Armstrong, J. Canales, P.G. Bruce, Angewandte Chemie International Edition 43 (2004) 2286–2288.
[20] R. Dominko, E. Baudrin, P. Umek, D. Arcon, M. Gaberscek, J. Jamnik, Electrochemistry Communications 8 (2006) 673–677.
[21] R. Dominko, L. Dupont, M. Gaberscek, J. Jamnik, E. Baudrin, Journal of Power Sources 174 (2007) 1172–1176.
[22] W.A. England, J.B. Goodenough, P.J. Wiseman, Journal of Solid State Chemistry 49 (1983) 289–299.
[23] S. Andersson, A.D. Wadsley, Acta Crystallographica 15 (1962) 194–201.
[24] A.L. Sauvet, S. Baliteau, C. Lopez, P. Fabry, Journal of Solid State Chemistry 177 (2004) 4508–4515.
[25] H. Rietveld, Acta Crystallographica 20 (1966) 508–513.
[26] H. Rietveld, Acta Crystallographica 22 (1967) 151–152.
[27] J. Rodriguez-Carvajal, Physica B: Condensed Matter 192 (1993) 55–69.
[28] S.Y. Yin, L. Song, X.Y. Wang, Y.H. Huang, K.L. Zhang, Y.X. Zhang, Electrochemistry Communications 11 (2009) 1251–1254.
[29] K. Zaghib, M. Armand, M. Gauthier, Journal of the Electrochemical Society 145 (1998) 3135–3140.
[30] Z. Yang, D. Choi, S. Kerisit, K.M. Rosso, D. Wang, J. Zhang, G. Graff, J. Liu, Journal of Power Sources 192 (2009) 588–598.
[31] E. Baudrin, S. Cassaignon, M. Koelsch, J.P. Jolivet, L. Dupont, J.M. Tarascon, Electrochemistry Communications 9 (2007) 337–342.
[32] J.C. Pérez Flores, A. Kuhn, F. García Alvarado, Nuevo electrodo anódico Li–Na–Ti–O para baterías recargables de litio y de ión litio, Patent ES 2 334 754, España (2009).
[33] Y.-J. Hao, Q.-Y. Lai, J.-Z. Lu, H.-L. Wang, Y.-D. Chen, X.-Y. Ji, Journal of Power Sources 158 (2006) 1358–1364.
[34] J. Gao, J. Ying, C. Jiang, C. Wan, Journal of Power Sources 166 (2007) 255–259.